Journal of Physics D: Applied Physics

PAPER • OPEN ACCESS

2D spatially resolved O atom density profiles in an atmospheric pressure plasma jet: from the active plasma volume to the effluent

To cite this article: David Steuer *et al* 2021 *J. Phys. D: Appl. Phys.* **54** 355204

OPEN ACCESS
IOP Publishing
Journal of Physics D: Applied Physics
J. Phys. D: Appl. Phys. 54 (2021) 355204 (12pp)
https://doi.org/10.1088/1361-6463/ac09b9

2D spatially resolved O atom density profiles in an atmospheric pressure plasma jet: from the active plasma volume to the effluent

David Steuer[1,*], Ihor Korolov[2], Sascha Chur[3], Julian Schulze[2,4], Volker Schulz-von der Gathen[3], Judith Golda[1] and Marc Böke[3]

[1] Plasma Interface Physics, Ruhr-University Bochum, D-44801 Bochum, Germany
[2] Department of Electrical Engineering and Information Science, Ruhr-University Bochum, D-44780 Bochum, Germany
[3] Experimental Physics II: Physics of Reactive Plasmas, Ruhr-University Bochum, D-44801 Bochum, Germany
[4] Key Laboratory of Materials Modification by Laser, Ion, and Electron Beams (Ministry of Education), School of Physics, Dalian University of Technology, Dalian 116024, People's Republic of China

E-mail: david.steuer@rub.de

Received 15 February 2021, revised 20 May 2021
Accepted for publication 9 June 2021
Published 22 June 2021

Abstract
Two-dimensional spatially resolved absolute atomic oxygen densities are measured within an atmospheric pressure micro plasma jet and in its effluent. The plasma is operated in helium with an admixture of 0.5% of oxygen at 13.56 MHz and with a power of 1 W. Absolute atomic oxygen densities are obtained using two photon absorption laser induced fluorescence spectroscopy. The results are interpreted based on measurements of the electron dynamics by phase resolved optical emission spectroscopy in combination with a simple model that balances the production of atomic oxygen with its losses due to chemical reactions and diffusion. Within the discharge, the atomic oxygen density builds up with a rise time of 600 μs along the gas flow and reaches a plateau of 8×10^{15} cm^{-3}. In the effluent, the density decays exponentially with a decay time of 180 μs (corresponding to a decay length of 3 mm at a gas flow of 1.0 slm). It is found that both, the species formation behavior and the maximum distance between the jet nozzle and substrates for possible oxygen treatments of surfaces can be controlled by adjusting the gas flow.

Keywords: atmospheric pressure microplasma jet, COST-Jet, phase resolved optical emission spectroscopy, two photon absorption laser induced fluorescence, plasma chemistry

(Some figures may appear in colour only in the online journal)

* Author to whom any correspondence should be addressed.

1. Introduction

Non-thermal micro atmospheric pressure plasma jets (μAPPJs) [1–6] have been attracting a high level of attention due to their applications such as the treatment (modification [7, 8], deposition [9, 10] or etching [11]) of temperature sensitive surfaces. These plasma devices are characterized by a non-equilibrium thermal state in which ions and neutrals remain at room temperature, while electrons reach energies of several thousand Kelvin, providing a wide range of chemical reactions. The key advantage of μAPPJs over low pressure plasmas is the fact that they can be used in open air without a vacuum system, allowing the cold effluent containing the reaction products to be applied directly to the surface to be treated.

Reactive atomic oxygen and nitrogen species (RONS) are one of the main focuses of recent studies, as they are important for medical plasma applications such as wound healing [12, 13] or cancer therapy [14, 15]. The key to these applications is the generation of reactive species within the active plasma volume of μAPPJs by using helium with an admixture (up to a few percent) of molecular gases such as oxygen [16–18], nitrogen [19, 20] or water vapor [21, 22]. To control and optimize the formation of RONS, besides the knowledge of the complex gas composition caused by chemical reactions, also an understanding of the production processes is necessary. The dissociation of the molecular gas is dominated by electron impact collisions [23]. Thus, the space and time-dependent electron dynamics must be identified and understood.

The electron power absorption dynamics in μAPPJs can take place in two different modes [20, 24–27]. Due to the number of collisions with neutrals at atmospheric pressure, the conductivity is very low. In order to maintain current continuity, a strong electric field is generated inside the plasma bulk, which accelerates electrons in the central region between the electrodes. This power absorption mechanism is called Ω-mode and occurs twice per period (during expansion and collapse of the sheath) at the times of maximum current. At higher powers, the discharge can transition to the Penning-mode. This mode can be divided into a direct and an indirect channel. In the direct channel, electrons generated by Penning ionization inside the sheaths are accelerated through the sheath into the plasma bulk, where they can excite or ionize atoms. In addition to electrons, Penning ionization also generates positive ions. These are accelerated onto the adjacent electrode and can generate secondary electrons there, which in turn are accelerated into the bulk (indirect channel).

Recent studies have shown that the generation of atomic oxygen [17, 18] and nitrogen species [28], as well as that of metastable atoms, e.g. helium [29], can be controlled by voltage waveform tailoring [30, 31]. Here, a series of consecutive harmonics of a fundamental frequency is used, resulting in an asymmetric driving voltage waveform. Adjusting this waveform allows the power absorption of electrons to be controlled both spatially and temporally, thus optimizing the generation of reactive species.

Classical μAPPJs are operated at a single radio frequency of 13.56 MHz. A reference source for the generation of reactive species is the COST micro plasma jet [5, 32]. It was developed within the European Cooperation for Science and Technology (COST) action MP1101 'Biomedical Applications of Atmospheric Pressure Plasmas' and is used by various working groups worldwide to ensure the comparability of research results. In such a plasma jet, the neutral gas flows through the active plasma region at a speed that is determined by its flow rate. When it enters the plasma, it is exposed to energetic electrons that can dissociate its molecular constituents and generate radicals. Depending on the gas flow and the discharge conditions it takes a particular (rise) time and distance for a given radical density to build up in the active plasma region. After this time/distance, the radical density does not change anymore inside the plasma region and is determined by a balance of sources and losses of this particle species. Precise knowledge of this rise time/distance is important for plasma source development, energy efficiency, and optimization. If the electrodes of a plasma jet are longer than the rise length of the reactive species, the electrodes could be shortened to save energy and, thus, make the source more efficient. On the other hand, electrodes should be at least long enough to allow the built-up of reactive species and achieve a maximum density of them. For the actual usage of μAPPJs, in addition to the formation inside the plasma, the decay of the reactive species in the effluent is crucial. To determine the optimal treatment distances and times for different surfaces and substrates, the density profile in the effluent must be known. An important research task is, therefore, to reveal the decay of reactive species densities in the effluent caused by recombination or other chemical reactions.

The knowledge of space resolved absolute density profiles of reactive species along the gas flow, especially of atomic oxygen, is limited to measurements performed in previous versions of the micro plasma jet with similar electrode configuration [33–36]. These devices were assembled with significantly less strict requirements for tightness and selection of the materials in gas or plasma contact compared to those defined for the COST micro plasma jet [5, 37]. Furthermore, power measurements were often limited to the readout at the generator or before matching units. In addition to measurements, there are various models that describe the production of atomic oxygen within the plasma [38, 39] or its destruction in the effluent [23, 38, 40], which could be verified and improved by novel measurements based on more defined conditions.

The aim of this paper is to investigate the rise of atomic oxygen densities in a He/O_2 plasma along the gas flow in the COST jet and to provide a deeper understanding of its formation. Two dimensionally resolved absolute oxygen densities are measured for different gas flows by using two photon absorption laser induced fluorescence (TALIF) spectroscopy. The observed density profiles are understood based on measurements of the spatio-temporal electron dynamics by phase resolved optical emission spectroscopy (PROES) in combination with basic model calculations. Furthermore, the decay behavior of atomic oxygen in the effluent is studied as well.

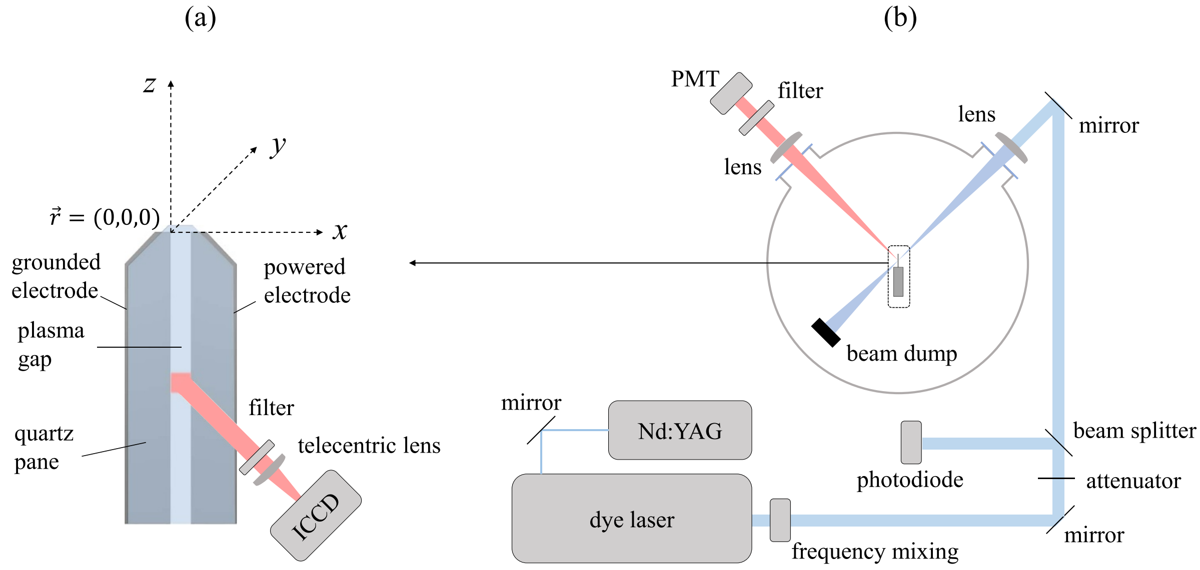

Figure 1. Sketch of the experimental set-up for the TALIF measurements. (a) COST jet including the used Cartesian coordinate system for the 2-dimensional density distributions. (b) Vacuum chamber and optical set-up.

The paper is structured as follows: in the next section, the experimental set-up is described, including the plasma source and the TALIF as well as the PROES set-up. The third section is divided into two subsections and presents the results of this work. First, the formation of atomic oxygen within the COST jet is investigated. In the second subsection, the effluent is studied. All results are compared to results of a simple model to describe the measured density profiles based on excitation rates determined experimentally via PROES measurements and including production, loss and diffusion terms. A conclusion is given in section 4.

2. Experimental set-up

2.1. Plasma source

Atomic oxygen measurements were performed in a μAPPJ, namely the COST jet. The capacitively coupled plasma is driven by a sinusoidal voltage waveform with a radio frequency (RF) of 13.56 MHz. The discharge volume is 30 mm $\times$ 1 mm $\times$ 1 mm and is enclosed between two identical stainless steel electrodes and two quartz plates that allow access for optical diagnostics. A sketch of the discharge channel is shown in figure 1(a). Further information about this plasma source including the power supply can be found elsewhere [5, 32]. Typically, the COST jet is operated with gas flows in the slm range. In this work we use 0.2–1.2 slm helium (purity 5.0) as feed gas flow which corresponds to a flow velocity of 3–20 m s^{-1}. In addition, a fixed admixture of oxygen (purity 4.8) of 0.5% is used, since previous studies have shown that the atomic oxygen density becomes maximum for this admixture [33, 36]. The dissipated plasma power can be determined by measuring the voltage, the current and their relative phase at the electrodes, through integrated probes, which are calibrated beforehand. The measurement of the dissipated power is described in more detail by Beijer *et al* [41]. The following results are obtained at a dissipated power of 1 W ($V_{rms} = 275$ V). The power was chosen because on the one hand as much oxygen as possible should be dissociated [23], but on the other hand the discharge should not switch to a constricted mode [5, 42], which would destroy the plasma source due to the high gas temperatures. At a power of 1 W, the gas temperature is approximately 350 K [5] and the plasma source can, therefore, also be used for biomedical treatments in the far effluent of the jet. Furthermore, powers of up to 1 W are commonly used, guaranteeing that the results are comparable to the literature [5, 19, 32, 43].

2.2. Diagnostics

A sketch of the experimental set-up is shown in figure 1 (b). The COST jet is mounted on a computer controlled XYZ stage (0.1 mm step resolution, custom made) facing upwards inside a vacuum chamber (51 cm diameter, 45 cm height). In order to compare spatial positions, we use a cartesian coordinate system with the origin located at the end of the grounded electrode at the jet nozzle shown in figure 1(a). To measure atomic oxygen densities within the plasma ($z \leqslant 0$ mm) as well as in the effluent ($z > 0$ mm) we use the TALIF technique [44, 45]. The laser system consists of a frequency doubled ns-pulsed Nd:YAG laser (Continuum Powerlite 8000, $\lambda = 532$ nm) pumping a tunable dye laser (Continuum ND6000). The Nd:YAG laser is triggered by a digital pulse generator (Stanford Research Systems DG535) at a repetition rate of 10 Hz. The oscillator of the dye laser is operated with a mixture of 63 mg pyridine 1 and 63 mg DSM in 1:l methanol, while the amplifier is operated with 28 mg DCM and 23 mg pyridine 1 in 1:l methanol. Its output radiation has a wavelength between 650 and 715 nm and can be tuned with a step resolution of 1 pm. To excite oxygen into the O (3p $^3P_{1,2,0}$)-state a wavelength of 224.31 nm is required. To obtain wavelengths in the UV range, the third harmonic of the dye laser frequency is generated by frequency mixing with a combination of a KD^*P (potassium dideuterium phosphate) and a BBO (beta barium borate) crystal. The UV laser beam has a diameter of about 3 mm and pulse energies of approximately 0.1 mJ. The laser pulse length is 6–7 ns. A beam splitter guides 8%–10% of the total power to a fast photo diode that monitors the beam energy. The remaining part is focused through a quartz lens ($f = 300$ mm) to the center of the vacuum chamber where the COST jet is placed. The local resolution is given by the full width at half maximum of the laser beam. It is determined to be 220 ± 20 μm. To avoid reflections of the laser a beam dump is installed inside the vacuum chamber. The fluorescence signal resulting from the de-excitation of atomic oxygen into the O (3 s ^{3}S)-state state is observed perpendicular to the laser beam at a wavelength of $\lambda = 844.87$ nm. A gated and cooled photo-multiplier (PMT, BURLE C31034A) measures the signal through a lens (BK7) and an interference filter (1.3 nm FWHM). As indicated in figure 1, the angle between the discharge channel and the laser beam respectively the fluorescence signal is 45 degrees. This configuration prevents coupling of the laser radiation into the PMT. However, reflections occur at the end of the quartz windows due to this angle, thus the first 2 mm of the effluent cannot be observed with this set-up. To avoid saturation effects, it must be ensured that the measured fluorescence signal depends linearly on the square of the laser intensity [45]. For this purpose, a computer-controlled dielectric attenuator is used, that consists of a dielectrically coated thin quartz plate and a stepper motor that controls the angle of the quartz plate relative to the laser beam. It is placed in front of the beam splitter so that the laser intensity can be varied without varying the operation conditions of the laser system and by this changing the properties of the laser pulse.

To determine absolute oxygen densities a calibration is required. The most common method is a noble gas calibration using xenon. For this method the optics of the TALIF set-up does not have to be changed, because both the two-photon resonance and the fluorescence wavelength of xenon are close to that of oxygen. The TALIF set-up and the calibration procedure are described in more detail elsewhere [18, 44]. Due to uncertainties of the constants used in the calibration procedure, the accuracy of the absolute densities presented here is better than 50%–60%. However, the experimental system is stable, allowing relative trends to be reproduced with a deviation of less than 20%.

To investigate the dynamics of energetic electrons, PROES measurements are performed as the basis of the model described below. These could be performed without modifications using the same experimental setup. To observe the helium emission line at 706.5 nm a fast ICCD camera (Andor iStar DH334T-18U-73) is equipped with a 40 mm telecentric lens (Edmund optics 4X CompactTL) and an interference filter (700 nm central wavelength, 15 nm FWHM). The camera is synchronized with the driving radio frequency voltage waveform by using a high voltage probe, that measures this voltage waveform, and a digital delay generator (Standford Research Systems DG645) that uses the measured waveform as a trigger input. Subsequently, it is used to set an adjustable delay with respect to a specific time within the RF period determined by the trigger signal. The temporal resolution is determined by the gate width of 3 ns. The electron impact excitation rate from the helium ground state into the He-I 1s3s $^3S_1$ level is calculated based on a collisional-radiative model which is described in more detail elsewhere [20, 28].

3. Results

3.1. Atomic oxygen formation along the gas flow

In the following, the formation of atomic oxygen along the direction of the gas flow and between the electrodes is investigated in the COST jet. Since the flow velocity determines the transit time through the discharge, the gas flow will be varied in the following. Gas flows from 0.2 to 1.2 slm helium are set in 0.2 slm steps. For the purpose of clarity, only the results of three gas flows are presented below. Figures 2(a)–(c) shows the measured 2D spatially resolved and time averaged atomic oxygen density for 0.2, 0.6 and 1.0 slm helium flow. The step size of the XYZ stage is set to 0.2 mm in the x-direction and to 1.0 mm in the z-direction. Here z describes the axis along the gas flow and x the distance between the electrodes (see figure 1(a)). The oxygen admixture is fixed at 0.5% and the power is set to 1 W. For each data point, the fluorescence signals of 64 laser shots are averaged. Overall, the distribution of atomic oxygen is symmetrically distributed between the electrodes (located at $x = 0$ mm and $x = 1$ mm, see figures 2(a)–(c)). The highest oxygen concentration is located in the center between the two electrodes and decreases towards the sides (perpendicular to the gas flow). In the direction of the gas flow, the oxygen density builds up and approaches a plateau at 8×10^{15} cm^{-3} (see also figure 4). While the maximum value is independent of the gas flow within the errors of the experimental system, its increase from the gas inlet at $z = -30$ mm to the position, where the plateau value is reached, differs significantly depending on the gas flow. At small helium flows of 0.2 slm a plateau is already reached within the first 10 mm. For larger flows such as 1.0 slm, the oxygen density increases until the end of the active plasma zone located at $z = 0$, so that no equilibrium state is reached at this point.

Since the production of atomic oxygen is mainly governed by the electron impact reactions in the used system [23], we measure the space and time resolved electron-impact excitation rate I_{exc} from the ground state of helium into He-3 s^3 S_1(22.7 eV) shown in figure 3 to trace energetic electrons as a basis for understanding the mechanisms of atomic oxygen formation. The measurements are taken under the same discharge conditions as those used for the previously presented TALIF measurements at $z = -15$ mm. At this position, a significant atomic oxygen density has already built up and the influence of the ambient air backflow through the gas outlet is negligible. During one RF-period four excitation maxima are observed. These can be traced back to different electron heating mechanisms, which each act once per half-period. Maxima (1) and (2) occur at the time of high current, when the sheath expands at the grounded electrode and collapses at

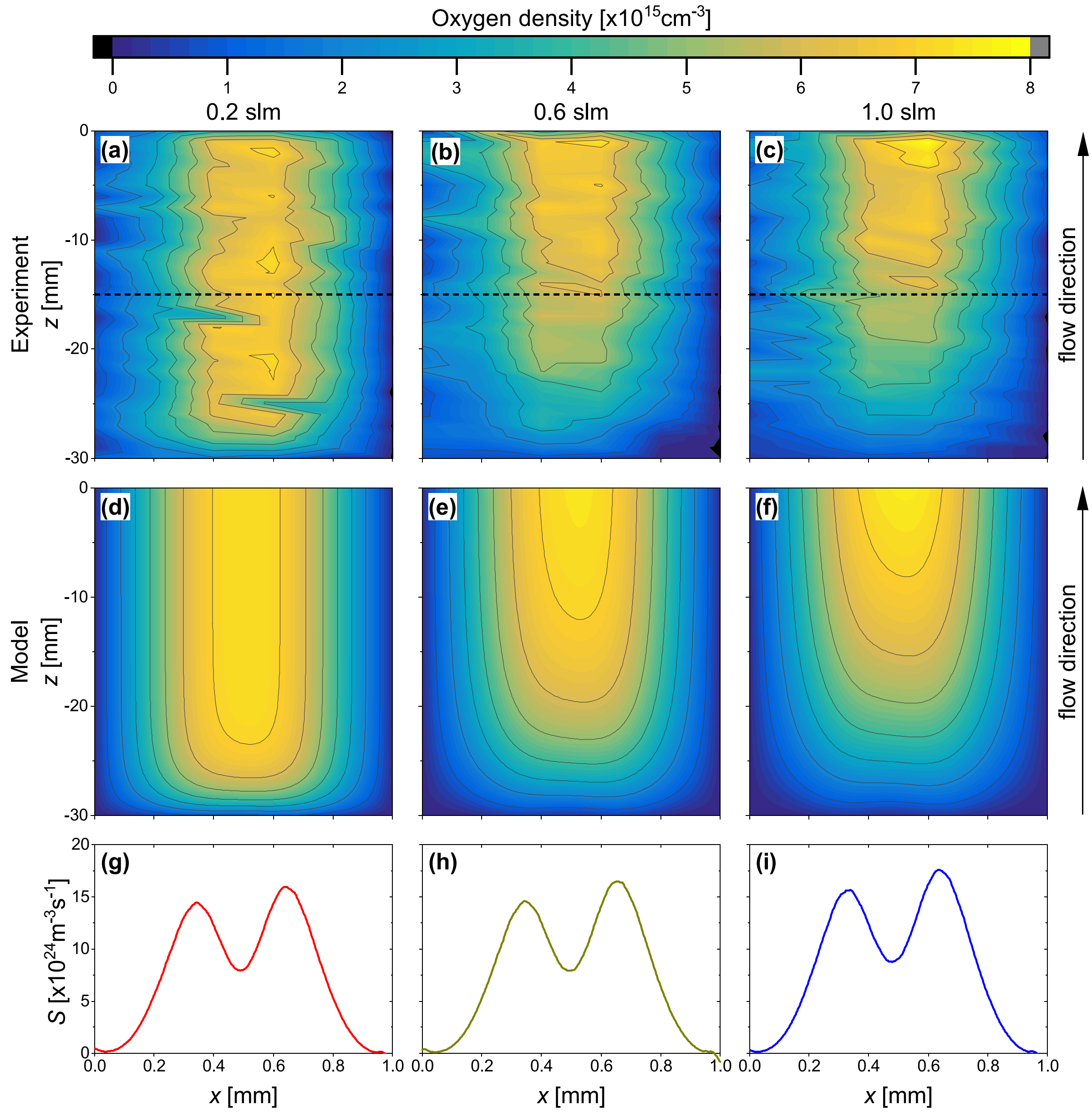

Figure 2. (a)–(f) 2D spatial distribution of the atomic oxygen density inside the COST jet measured by TALIF (a–c) and obtained from the model (d–f). The dashed line indicates the position of the PROES measurements described below. (g–i) Spatially resolved atomic oxygen production rate determined from equation (7). The flow direction is indicated by the arrow on the right. Discharge conditions: He + 0.5% O_2 admixture at a power of 1 W.

the powered electrode. At this time within the RF period, the observed excitation pattern is similar to the electron dynamics observed in low pressure electronegative CCPs [30, 46], where electrons are accelerated by the combination of a strong drift electric field in the plasma bulk and ambipolar electric fields on the bulk side of the sheath edges. The profile of the electric field in the direction perpendicular to the electrodes ensures current continuity in the presence of an inhomogeneous profile of the electron density and, thus, the conductivity. The high drift field is caused by a depleted conductivity due to the high collisionality at atmospheric pressure and the electronegativity that depletes the electron density. The ambipolar field is a consequence of local gradients of the electron density profile. In electronegative CCPs local maxima of the electron density can occur in the electropositive edge region of the plasma. Maximum (3) is caused by electrons generated inside the sheath via Penning ionization as a consequence of helium metastables. In this way electrons are generated inside the sheath and accelerated into the plasma bulk by the sheath electric field, where they can cause excitation and ionization. Ions produced during Penning ionization are accelerated to the adjacent electrode where they can produce secondary electrons. These electrons are then accelerated into the plasma bulk and can also cause excitation and ionization. It is noticeable that the excitation in front of the powered electrode ($x = 1$ mm) is slightly stronger (about 10%) than in front of the grounded electrode ($x = 0$ mm). This can be attributed to an extra grounded shielding near the grounded electrode, which affects the electric field by making the plasma source slightly asymmetric.

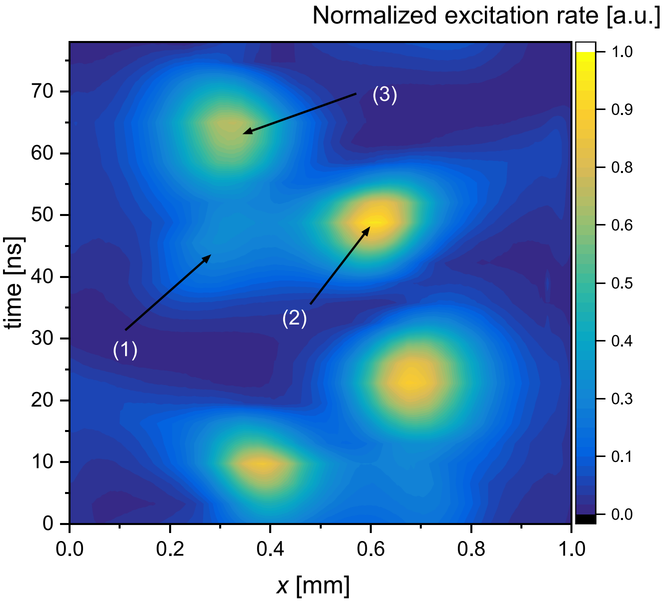

Figure 3. Spatio-temporal plots of the electron impact excitation rate from the ground state into the He-I 1s3s $^3S_1$ level at $z = -15$ mm. All values are normalized to the maximum. The coordinate x describes the distance between the grounded electrode ($x = 0$ mm) and the powered electrode ($x = 1$ mm). Discharge conditions: 0.6 slm He + 0.5% O_2 admixture at a power of 1 W.

The electron-impact excitation rate measurements were performed for all applied gas flows. Since the changes between the measurements are small, only one example is shown in figure 3 for reasons of clarity. All in all, certain differences in the intensity of the excitation, especially in region 3, can be identified between the three gas flows, which can be attributed to a change in the gas composition. The PROES measurements are all performed at the same position ($z = -15$ mm). As shown above, the atomic oxygen density builds up differently depending on the helium flow. This means that as long as no state of equilibrium has been reached with a specific gas flow, the gas composition at this position is different. Based on the TALIF measurements presented here, the atomic oxygen density differs by about 20% between the 0.2 and 1.0 slm gas flows at the position $z = -15$ mm. Further changes of the chemical composition depending on the gas flow can be induced by processes such as the production of ozone which consumes both atomic and molecular oxygen. A consequence of this is a decrease in the excitation rate of the Penning-mode with increasing gas flows. This is consistent with measurements of Bischoff *et al* [20] where a transition from the Penning-mode to the Ω-mode was observed at higher nitrogen admixtures. This behavior could be attributed to an increase in collisions of electrons with the molecular gas and, thus, to a stronger electric field in the plasma bulk. In our case, the oxygen admixture remains constant at 0.5%. However, the dissociation degree of molecular oxygen decreases with the gas flow, resulting in an increase of the molecular oxygen fraction at the position $z = -15$ mm.

For the discharge conditions used here (helium + 0.5% O_2) atomic oxygen is produced mainly by electron impact dissociation [23]:

$$e^- + O_2 \rightarrow O + O + e^- \tag{1}$$

$$\rightarrow O + O(^1D) + e^-. \tag{2}$$

Oxygen metastables are mainly destructed by helium:

$$O(^1D) + He \rightarrow O + He. \tag{3}$$

The cross sections of these reactions shown above have the maximum between 19 and 50 eV [47, 48]. Thus, the source of atomic oxygen $S(x,t)$ can be roughly assumed to be proportional to the electron impact excitation of helium atoms from the ground state into He-I 1s3s $^3S_1$ (excitation threshold energy: 22.7 eV) shown in figures 3(a)–(c) and discussed above. In order to describe the atomic oxygen density $n(x,t)$ by a simple model, not only the production rate $S(x,t)$ but also the loss rate $L(x,t)$ and the diffusion of atomic oxygen to the walls and electrodes must be considered. The losses are dominated by 3-body recombination, which leads to the production of ozone [23]:

$$O + O_2 + He \rightarrow O_3 + He. \tag{4}$$

The atomic oxygen density can now be predicted by solving the following equation based on Ficks's second law:

$$\frac{\partial n(x,t)}{\partial t} = D\frac{\partial^2 n(x,t)}{\partial x^2} + S(x,t) - L(x,t). \tag{5}$$

The losses L(x,t) result from the reaction rate $k_L = 3.0 \times 10^{-46}(300/T_g^{2.6})\ m^6 s^{-1}$ [49, 50] of equation (4) and the density of helium n_{He} and molecular oxygen n_{O_2}, which are assumed to be constant:

$$L(x,t) = k_L n(x,t) n_{O_2} n_{He}. \tag{6}$$

The diffusion of atomic oxygen can be described by the diffusion coefficient $D_O = 1.29 \times 10^{-4}\ m^2\ s^{-1}$ [23]. To convert the measured electronic impact excitation, I_{exc}, into a production rate $S(x,t)$, a proportionality constant κ is necessary. Since an RF-period is significantly shorter than the reaction times of the processes mentioned above, it is reasonable to consider the time average of the excitation.

$$S(x) = \kappa \langle I_{exc}(x) \rangle_t. \tag{7}$$

The parameter κ is adjusted in a way that the calculated value of the atomic oxygen density corresponds to the measured maximum atomic oxygen density at $z = 0$ mm. Its value increases linearly with the gas flow from 0.2 to 1.0 slm by

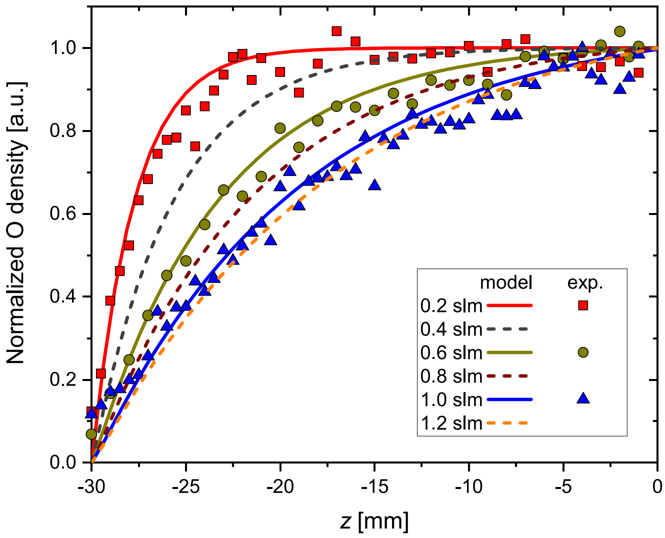

Figure 4. 1D spatial distribution of the atomic oxygen density inside the COST jet measured by TALIF and obtained from the numerical solution of (equation (5)) at $x = 0.5$ mm. Discharge conditions: He + 0.5% O_2 admixture at a power of 1 W.

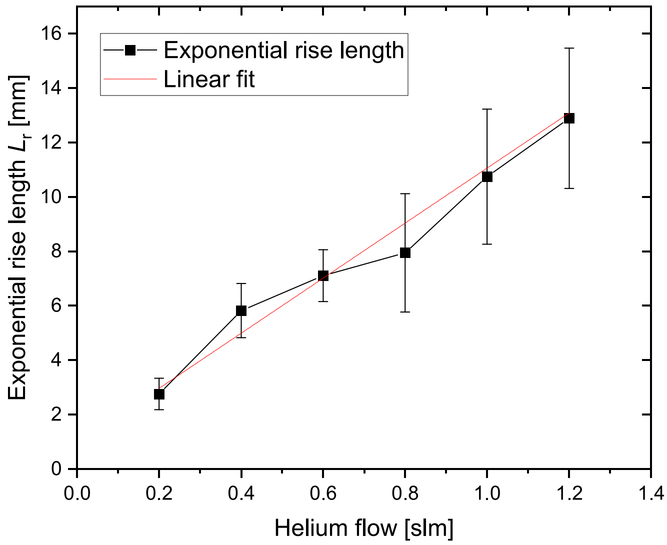

Figure 5. Exponential rise lengths L_r of atomic oxygen depending on the helium gas flow obtained by using equation (10) as fitting function at $x = 0$ mm. Discharge conditions: He + 0.5% O_2 admixture at a power of 1 W.

a total of 20%. This increase can be explained by different gas compositions at the position ($z = -15$ mm) at different flows and the resulting different electron energy distribution functions (EEDFs). The calculated production rates, S, are presented in figures 2(g)–(i). As known from the PROES measurements, the excitation takes place mainly at the sheath edges. This results in a characteristic oxygen production profile with two peaks. The stronger excitation in front of the powered electrode (about 10%) is also reflected in the production rate. The absolute values of the production rate are in the order of 10^{25} m^{-3} s^{-1} (comparable to previous simulations of Waskoenig *et al* [23]) and increase with the gas flow by a total of 10%.

To solve equation (5) boundary conditions are necessary. At the positions $x = 0$ mm and $x = 1$ mm an atomic oxygen surface loss coefficient β is used, which is defined by the ratio of the outgoing flow, Γ_{out}, to the incident flow, Γ_{in}:

$$\beta = 1 - \frac{\Gamma_{out}}{\Gamma_{in}}. \tag{8}$$

In this paper we use $\beta = 0.07$ which was determined experimentally for stainless steel electrodes [51]. The losses on the quartz plates can be neglected due to a low value for β (10^{-4} to 10^{-3}) [52–54]. Furthermore, it is assumed that the atomic oxygen density at the position $z = -30$ mm (gas inlet) equals to zero. Equation (5) can be solved numerically by an explicit Euler forward approximation. The solution is illustrated in figures 2(d)–(f). To use the model with the coordinate system shown in figure 1(a), the time t can be converted to a position z assuming a constant gas velocity:

$$z = \frac{\Phi_{\mathrm{He}}}{A} t - 30 \text{ mm}, \tag{9}$$

where Φ_{He} is the gas flow and $A = 1$ mm^2 is the entrance surface area of the jet channel. Both, the two-dimensional distribution of the atomic oxygen density as well as its absolute values obtained from this model are in close agreement with the TALIF measurements (figures 2(a)–(c)).

The very good agreement between model and measurement is especially visible in the one-dimensional representation shown in figure 4, in which the atomic oxygen density at the centre between the electrodes ($x = 0.5$ mm) is plotted as a function of position in the direction along the gas flow. The measured exponential formation behavior is reproduced by the model.

The formation length L_r of atomic oxygen characterizes the rising behavior and can be determined by an exponential fit (equation (10)) to the measurement. The parameter a describes the maximum achievable atomic oxygen density:

$$f(z) = -a\left[\exp\left(-\frac{z+30}{L}\right) - 1\right]. \tag{10}$$

The formation length rises with increasing gas flow, as the average gas velocity increases and, therefore, the gas transit time through the gas channel decreases. Therefore, it is reasonable to convert the exponential formation length L_r into a rise time τ by including the gas flow and the cross-sectional area A:

$$\tau(L_r) = \frac{L_r \cdot A}{\Phi_{\mathrm{He}}}. \tag{11}$$

The results are illustrated in figure 5. The exponential rise length L_r increases linearly with the helium gas flow (0.2–1.2 slm) and is between 2.8 and 12.9 mm. The error bars represent the uncertainties of the respective exponential fits. A slope of 10 mm slm^{-1} follows from a linear fit. This can be converted into a rise time of 600 μs. The constant rise time shows that the production of atomic oxygen is dominated by electron impact processes and that the EEDF does not change due to the increased gas flow. It follows that the formation behavior of atomic oxygen can be adjusted directly via the gas flow. In a previous paper, Knake *et al* [35] determined this slope to be 1 mm slm^{-1} with an oxygen admixture of 0.6% and a generator power of 16 W. This results in a rise time of 60 μs. The differences can be explained by two effects. First, for the previous version of the plasma jet, only the applied power (set at the generator) could be measured, but not the actual dissipated power. From the publication it appears that the discharge at 16 W is about to switch to a constricted mode. In contrast, the COST jet in this paper is operated at 1 W and does not switch to a constricted mode until approximately 3 W [55]. Thus, it can be assumed that the dissipated power in our work is significantly lower than that used in the work of Knake *et al* [35]. As also shown in that work [35], a higher power leads to a smaller formation length. Second, the previous version of the jet and its gas tubing (plastics) were not as gas and humidity tight as the actual set-up that follows the procedures defined for the COST-jet [5]. This may have lead to impurities and, thus, to a different gas composition.

The results obtained here are important for optimizing the COST jet for various applications. By knowing the maximum atomic oxygen density at the end of the discharge channel, treatment times can be specified. The design of the COST jet is suitable for the gas flows used in this work. If gas flows of more than 1.0 slm are required, for example, for a higher output of reactive species, an extended version of the jet could offer advantages in the future.

3.2. Atomic oxygen densities in the effluent

For applications it is particularly important to know the reactive species density profile in the effluent to determine an adequate distance of substrates from the jet nozzle for treatment by reactive species generated by the jet. Outside the active plasma zone, any processes induced by energetic electrons are absent, resulting in a decay of the reactive species density through chemical reactions as a function of distance from the nozzle. The decay length L_d determines the treatment time and the optimal distance in which samples can be placed. Therefore, the spatial distribution of atomic oxygen in the effluent is studied in this section. Since the gas flow affects the effluent, it is varied again in the following.

In figures 6(a)–(c) two dimensional TALIF measurements of the atomic oxygen density in the effluent at different helium flows are shown. For a gas flow of 0.2 slm (figure 6(a)), the measurement was performed only up to a position of $z = 5.5$ mm, since the signal was already in the detection limit and therefore, no data is available for higher distances. Due to the experimental limitations mentioned above, the first 2 mm of the effluent cannot be captured. The step resolution in x- and z-direction is 0.2 and 0.3 mm, respectively. The average of the fluorescence signals of 64 laser shots is taken. A noble gas calibration was also carried out for the effluent. However, the calibration factor depends on the gas composition, as the quenching coefficients for the excited oxygen state are species dependent. While at the jet nozzle ($z = 0$ mm) it can be assumed that the gas composition corresponds to the set gas mixture, the influence of the ambient air becomes greater with an increasing z-position. Especially off the central axis ($x = 0.5$ mm) of the effluent, ambient air intrudes into the gas flow and significantly changes the gas composition. For this reason, the measurements are shown in a normalized way.

As already known from measurements inside the jet, the maximum oxygen density is located in the center between the two electrodes and decreases towards these boundary surfaces. In the direction of the gas flow, the oxygen density decreases exponentially due to the absence of electron impact collision sources, the formation of ozone and the interaction with other species in the expanding gas. The higher the gas flow is set, the further away from the outlet atomic oxygen is detectable. While with 0.2 slm the signal already decreased to 10% within 4 mm from the nozzle, atomic oxygen densities at 1.0 slm can be detected after more than 10 mm. The average absolute atomic oxygen density behind the jet outlet at $z = 3$ mm is 5×10^{15} cm^{-3}. This value is in agreement with previous measurements at the same position by Willems *et al* [36] who determined this density to be 4×10^{15} cm^{-3} for comparable parameters ($V_{rms} = 275$ V, 1.4 slm He + 0.6% O_2; here: $V_{rms} = 275$ V, 1.0 slm + 0.5% O_2) using TALIF and molecular beam mass spectrometry. The small differences in the oxygen admixture can be neglected, since the maximum oxygen density is reached at admixtures between 0.5% and 0.6% [33, 36].

For comparison the results of the model are presented in figures 6(d)–(f). The model can reproduce the general behavior in the effluent, although there are some differences. On the one hand, the model estimates the range of atomic oxygen to be too high and the density decreases much more slowly compared to the measured ones. On the other hand, the two-dimensional shape of the effluent also differs. While the measurement shows a rather triangular like shape, the model shows a more Gaussian like shape. These differences can be traced back to a number of simplifications of the model. First, the model assumes that the source term $S(x,t)$ (equation (7)) is switched off after $z = 0$ mm, because no atomic oxygen can be produced in this area by electron impact, neglecting that the effective production rate of atomic oxygen already includes losses. These losses may also play a role in the effluent, but are not accounted by the model. Secondly, the model assumes a laminar gas flow with a constant gas velocity between the electrodes. Inside the jet, this assumption was valid, however, the helium gas flow is slowed down as soon as it encounters the ambient air.

A one-dimensional (at $x = 0.5$ mm) logarithmic representation of the results is shown in figure 7. Here, the exponential decrease of the measured atomic oxygen density in the effluent is visible as well as the deviation between experiment and model. For this reason the simple model is extended to include Stokes friction. The equation of motion can be written as:

$$m\frac{\partial^2 z(t)}{\partial t^2} + \alpha\frac{\partial z(t)}{\partial t} = 0. \qquad (12)$$

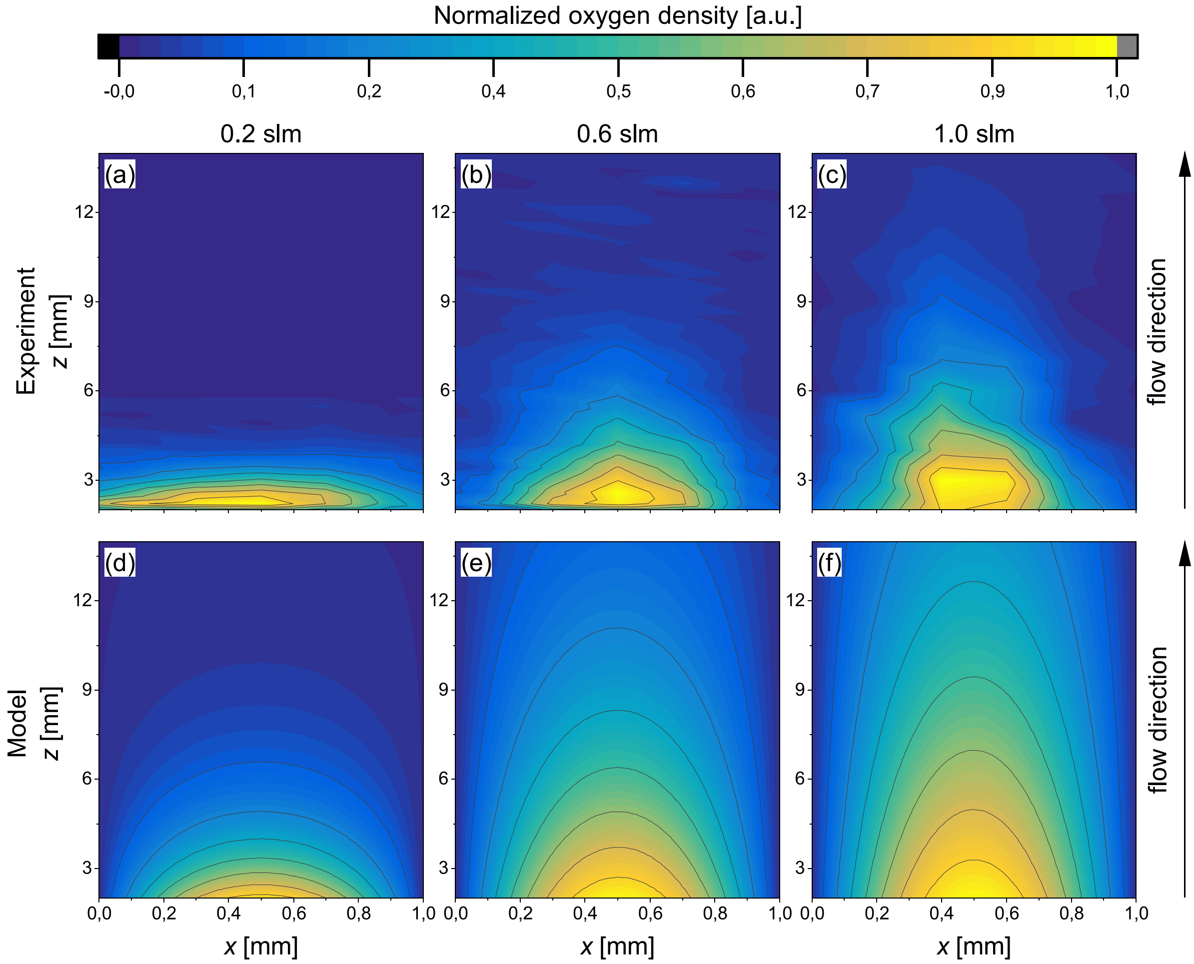

Figure 6. (a)–(f) 2D spatial distribution of the atomic oxygen density in the effluent of the COST jet measured by TALIF ((a)–(c)) and obtained from the numerical solution of equation (5) ((d)–(f)). The flow direction is indicated by the arrow on the right. Discharge conditions: He + 0.5% O_2 admixture at a power of 1 W.

Here $\alpha = 6\pi r\eta$ describes the Stokes friction coefficient with the dynamic viscosity η and the radius of a spherical particle r. By assuming a constant gas velocity V_0 at the point $z = 0$ mm, which results from the set gas flow, the equation can be solved:

$$z(t) = V_0 \Xi \left[1 - \exp\left(-\frac{t}{\Xi} \right) \right]. \tag{13}$$

The parameter $\Xi = m/\alpha$ was determined by Preissing *et al* [19] under comparable conditions to be 3.5×10^{-3} s. The equation of motion neglects gravitational and buoyancy effects. In fact, the orientation of the jet (e.g. upwards vs. downwards) should affect the oxygen density in the effluent via the buoyancy of helium. If the jet points upwards, the velocity of the helium atoms will be increased, while it will be decreased, if the jet points downwards. This will affect the oxygen density distribution, since oxygen atoms follow the helium flow. This was observed by Preissing *et al* for NO particles in a helium flow and based on a horizontal orientation of the jet [19]. To study this effect, the orientation of the jet would have to be changed systematically. This is, unfortunately, not possible in our experiment and beyond the scope of this work.

As a result, the gas velocity in the effluent is no longer constant, but decreases as a function of distance from the jet nozzle. The extended model is closer to the experiment than the simple model. Especially the behavior at low gas flows (0.2 slm) can be reproduced. Nevertheless, the deviation at higher gas flows is still significant. One explanation for this is the intrusion of ambient air into the helium flow, which was studied by Preissing *et al* [19]. Here, the initial gas composition changes due to the penetration of ambient air in the effluent. This change can have an impact on the TALIF measurements, because the TALIF calibration is based on a fixed gas composition since the radiation-less de-excitation (quenching) must be estimated. This challenge was overcome by Klose *et al* [56] using a ps-laser that could directly measure the effective lifetime of the excited oxygen state. However, in our work, ns-laser pulses were used which are not able to resolve the decay of the fluorescence signal. Thus, the effective lifetime had to be calculated on the basis of the gas mixture. If a fraction of molecular nitrogen is added, excited oxygen atoms are quenched more strongly [44], resulting in lower fluorescence

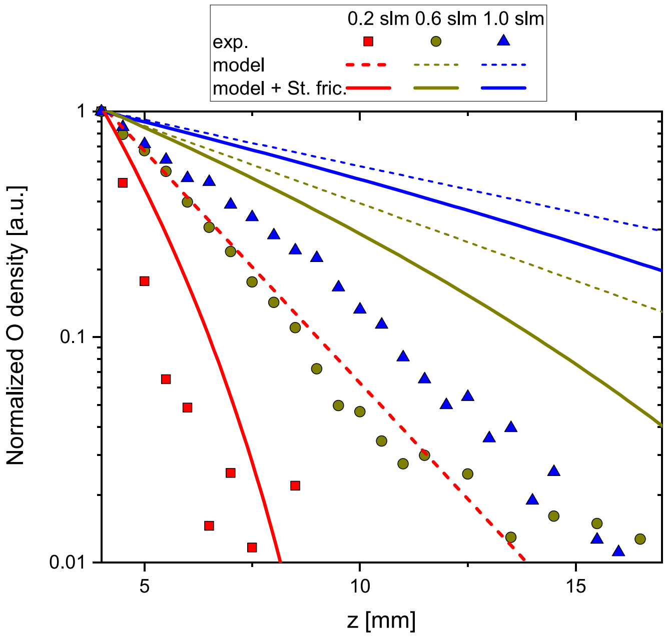

Figure 7. 1D spatial distribution of the atomic oxygen density in the effluent of the COST jet measured by TALIF and obtained from the numerical solution of equation (5) and an extended model that includes Stokes friction at $x = 0.5$ mm. Discharge conditions: He + 0.5% O_2 admixture at a power of 1 W. For each gas flow the atomic oxygen density is normalized by its value at $z = 4$ mm.

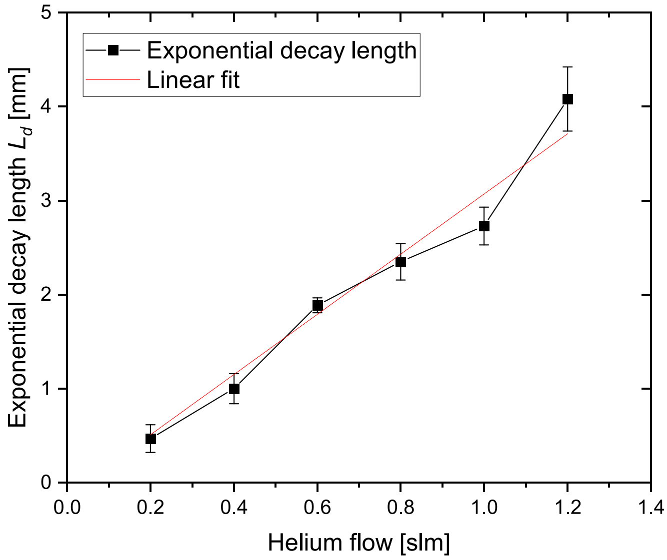

Figure 8. Exponential decay lengths, l_d, of atomic oxygen as a function of the helium flow obtained by using equation (10) as fitting function at $x = 0.5$ mm. Discharge conditions: He + 0.5% O_2 admixture at a power of 1 W.

signals. Accordingly, the real oxygen density is higher than the measured density, especially at greater distances, and thus closer to the model. This effect also explains the triangular shape of the oxygen distribution, as the air penetrates from the outside to the inside. If the effluent entered a defined helium atmosphere instead of ambient air, it would be expected that both the decay length and the two-dimensional shape could be reproduced by the model [19]. Furthermore, the model only considers one loss reaction ($He + O + O_2 \rightarrow He + O_3$). In reality, further reactions can take place, for example in combination with ozone ($O + O_3 \rightarrow 2O_2$) and reduce the atomic oxygen density.

To further characterize the decay of the atomic oxygen density in the effluent, the exponential decay length, l_d, can be determined. Equation (14) can be used as a fitting function for this purpose. Here A is an arbitrary constant and y_e is the background signal in the effluent:

$$f(z) = A \exp\left(-\frac{z}{L_d}\right) + y_e. \quad (14)$$

The results are illustrated in figure 8. As observed before, the decay length increases with the gas flow, since oxygen atoms can travel further distances in the same time due to the higher gas velocities. Small deviations from a linear behavior, especially at large gas flows, show that the case of a laminar flow exists only conditionally. As previously discussed, the effluent is strongly influenced by friction (resulting in a changing gas velocity) and intrusion of ambient air into the gas flow of the jet. Therefore, it is only meaningful to define a decay time on the central axis ($x = 0$ mm), which is 180 μs. From measurements of the decay length by Knake *et al* using the previous version of the micro plasma jet, a decay time of 120 μs is obtained. The difference can be traced back to impurities, as already described above. If a small concentration of nitrogen or humidity is already present in the discharge channel, it also remains in the effluent and can contribute to the non-radiative de-excitation of oxygen atoms, which leads to a shorter decay time. The design and materials used in the COST jet have significantly reduced the impurities, preventing nitrogen and humidity from contributing to the de-excitation until ambient air enters the effluent, resulting in an increased decay time in the COST jet.

All in all, the measurements show that the effluent can be controlled by the gas flow. Based on these results, both, treatment distances and treatment times can be adjusted and optimized for a wide range of applications. In general, the treatment range can be maximized by increasing the gas flow. However, if the gas flow is too high, the maximum oxygen density can no longer be produced within the discharge. A compromise between a sufficient gas flow and optimum oxygen production is a gas flow of 1.0 slm, which allows treatment ranges of over 10 mm to be achieved. For higher gas flows, a jet with longer electrodes could be used.

4. Conclusion

The formation of atomic oxygen along the gas flow in a He/O_2 µAPPJ and its decay in the effluent was studied. Spatially resolved measurements of the atomic oxygen density were performed using TALIF spectroscopy. For this purpose, the helium gas flow was varied from 0.2 to 1.2 slm in 0.2 slm steps with a constant oxygen admixture of 0.5%. The results could be reproduced and understood by a combination of a model and the spatio-temporal electron impact excitation rates from the ground state into He-I 1s3s $^3S_1$ measured by PROES.

The distribution of atomic oxygen within the COST jet was investigated by two-dimensional measurements. The atomic oxygen density reaches values of up to 8×10^{15} cm^{-3} independently of the gas flow. The maximum density is concentrated in the center between the two electrodes and increases along the gas flow. At low gas flows, the density builds up very steeply, once the gas enters the active plasma volume, and reaches a plateau (at a gas flow of 0.2 slm this happens within 10 mm). In contrast, the density increases less steeply at higher flows and no equilibrium state can be reached inside the COST jet.

PROES measurements show that, at the plasma parameters used here, the COST jet operates in a hybrid electron power absorption mode in which bulk electrons are accelerated by high electric fields in the bulk at the times of high current and secondary electrons generated via Penning ionization are accelerated towards the bulk by the sheath electric field. Both groups of electrons can cause excitation and dissociation of the background gas. This leads to a production rate of atomic oxygen with two peaks near the sheath edges. A model combines this production of atomic oxygen with losses through chemical reactions and diffusion. This allowed the density measurements, especially the build-up of the atomic oxygen density, to be reproduced and understood.

The formation of atomic oxygen can be further described by determining the exponential rise length, which increases with the gas flow. From the linear behavior a constant rise time of 600 μs can be determined.

In addition to the behavior within the plasma, the effluent was investigated. Here, the atomic oxygen density decays exponentially as a function of distance from the jet nozzle. This is due to the fact that production by electron impact dissociation takes place only within the plasma, but atomic oxygen continues to be consumed by chemical reactions such as the formation of ozone in the effluent. By increasing the gas flow and the associated gas velocity, the treatment range of a substrate by atomic oxygen can be significantly extended (more than 10 mm at 1.0 slm helium). Similar to the exponential rise length within the discharge, the exponential decay length increases with the gas flow. The decay time is 180 μs. The 2D spatially resolved atomic oxygen distribution shows a triangle-like shape in the effluent. To further understand the behavior of the effluent, future measurements with surfaces to be treated will help to include material-dependent surface losses and shielding phenomena.

In this work the COST jet was investigated with regard to applications based on He/O_2 plasmas. With the help of the parameters found here, both the formation of atomic oxygen within the discharge and the treatment range in the effluent can be adjusted and controlled with the help of the tunable gas flow. The agreement between measurements and model calculations shows that a simple model can be used to make predictions about the behavior of the COST jet. Increasing the gas flow allows to increase the treatment distance as long as the residence time of the gas in the active plasma volume is sufficiently high to generate a high atomic oxygen density. In the present setup, i.e. for the present length of the jet, a compromise between high oxygen production and long treatment range can be found at a flow of 1.0 slm. For applications with low gas flows, energy could be saved by using shorter electrodes, whereas for applications with gas flows greater than 1.0 slm, an extended version is useful to maximize oxygen production. This may provide a simple and easy to use basis for up-scaling of applications of the COST jet and similar devices.

Data availability statement

The data that support the findings of this study are available upon reasonable request from the authors.

Acknowledgment

This work is supported by the DFG via SFB 1316 (Projects A4 and B2).

ORCID iDs

David Steuer https://orcid.org/0000-0003-3005-0829
Ihor Korolov https://orcid.org/0000-0003-2384-1243
Sascha Chur https://orcid.org/0000-0001-6926-3747
Julian Schulze https://orcid.org/0000-0001-7929-5734
Volker Schulz-von der Gathen https://orcid.org/0000-0002-7182-3253
Judith Golda https://orcid.org/0000-0003-2344-2146
Marc Böke https://orcid.org/0000-0003-1062-5808

References

[1] Lu X, Laroussi M and Puech V 2012 *Plasma Sources Sci. Technol.* **21** 034005
[2] Winter J, Brandenburg R and Weltmann K D 2015 *Plasma Sources Sci. Technol.* **24** 064001
[3] Robert E, Sarron V, Riès D, Dozias S, Vandamme M and Pouvesle J M 2012 *Plasma Sources Sci. Technol.* **21** 034017
[4] Sobota A *et al* 2016 *Plasma Sources Sci. Technol.* **25** 065026
[5] Golda J *et al* 2016 *J. Phys. D: Appl. Phys.* **49** 084003
[6] Reuter S, von Woedtke T and Weltmann K D 2018 *J. Phys. D: Appl. Phys.* **51** 233001
[7] Pawlat J, Terebun P, Kwiatkowski M and Diatczyk J 2016 *J. Phys. D: Appl. Phys.* **49** 374001
[8] Shaw D, West A, Bredin J and Wagenaars E 2016 *Plasma Sources Sci. Technol.* **25** 065018
[9] Benedikt J, Raballand V, Yanguas-Gil A, Focke K and von Keudell A 2007 *Plasma Phys. Control. Fusion* **49** B419–27
[10] Reuter R, Rügner K, Ellerweg D, de los Arcos T, von Keudell A and Benedikt J 2012 *Plasma Processes Poly.* **9** 1116–24
[11] Ichiki T, Taura R and Horiike Y 2004 *J. Appl. Phys.* **95** 35–9
[12] Graves D B 2014 *Phys. Plasmas* **21** 080901
[13] Kong M G, Kroesen G, Morfill G, Nosenko T, Shimizu T, van Dijk J and Zimmermann J L 2009 *New J. Phys.* **11** 115012
[14] Graves D B 2014 *Plasma Processes Poly.* **11** 1120–7
[15] Yang H, Villani R M, Wang H, Simpson M J, Roberts M S, Tang M and Liang X 2018 *J. Exp. Clin. Cancer Res.* **37** 266

[16] Maletić D, Puač N, Lazović S, Malović G, Gans T, Schulz-von der Gathen V and Petrović Z L 2012 *Plasma Phys. Control. Fusion* **54** 124046
[17] Liu Y*et al* 2020 Micro atmospheric pressure plasma jets excited in He/O_2 by voltage waveform tailoring: A study based on a numerical hybrid model and experiments *Plasma Sources Sci. Technol.* (https://doi.org/10.1088/1361-6595/abd0e0)
[18] Korolov I, Steuer D, Bischoff L, Hübner G, Liu Y, Schulz-von der Gathen V, Böke M, Mussenbrock T and Schulze J 2021 *J. Phys. D: Appl. Phys.* **54** 125203
[19] Preissing P, Korolov I, Schulze J, Schulz-von der Gathen V and Böke M 2020 *Plasma Sources Sci. Technol.* **29** 125001
[20] Bischoff L *et al* 2018 *Plasma Sources Sci. Technol.* **27** 125009
[21] Benedikt J, Schröder D, Schneider S, Willems G, Pajdarová A, Vlček J and Schulz-von der Gathen V 2016 *Plasma Sources Sci. Technol.* **25** 045013
[22] Willems G, Benedikt J and von Keudell A 2017 *J. Phys. D: Appl. Phys.* **50** 335204
[23] Waskoenig J, Niemi K, Knake N, Graham L M, Reuter S, Schulz-von der Gathen V and Gans T 2010 *Plasma Sources Sci. Technol.* **19** 045018
[24] Schulz-von der Gathen V, Schaper L, Knake N, Reuter S, Niemi K, Gans T and Winter J 2008 *J. Phys. D: Appl. Phys.* **41** 194004
[25] Liu D W, Iza F and Kong M G 2008 *Appl. Phys. Lett.* **93** 261503
[26] Liu D W, Iza F and Kong M G 2009 *Appl. Phys. Lett.* **95** 031501
[27] Hemke T, Eremin D, Mussenbrock T, Derzsi A, Donkó Z, Dittmann K, Meichsner J and Schulze J 2012 *Plasma Sources Sci. Technol.* **22** 015012
[28] Korolov I, Donkó Z, Hübner G, Bischoff L, Hartmann P, Gans T, Liu Y, Mussenbrock T and Schulze J 2019 *Plasma Sources Sci. Technol.* **28** 094001
[29] Korolov I *et al* 2020 *J. Phys. D: Appl. Phys.* **53** 185201
[30] Brandt S *et al* 2016 *Plasma Sources Sci. Technol.* **25** 045015
[31] Schulze J, Schuengel E, Donko Z and Czarnetzki U 2010 *Plasma Sources Sci. Technol.* **19** 045028
[32] Riedel F *et al* 2020 *Plasma Sources Sci. Technol.* **29** 095018
[33] Knake N, Reuter S, Niemi K, Schulz-von der Gathen V and Winter J 2008 *J. Phys. D: Appl. Phys.* **41** 194006
[34] Knake N, Niemi K, Reuter S, Schulz-von der Gathen V and Winter J 2008 *Appl. Phys. Lett.* **93** 131503
[35] Knake N and Schulz-von der Gathen V 2010 *Eur. Phys. J.* D **60** 645–52
[36] Willems G, Golda J, Ellerweg D, Benedikt J, von Keudell A, Knake N and Schulz-von der Gathen V 2019 *New J. Phys.* **21** 059501
[37] Winter J, Wende K, Masur K, Iseni S, Dünnbier M, Hammer M U, Tresp H, Weltmann K D and Reuter S 2013 *J. Phys. D: Appl. Phys.* **46** 295401
[38] Hemke T, Wollny A, Gebhardt M, Brinkmann R P and Mussenbrock T 2011 *J. Phys. D: Appl. Phys.* **44** 285206
[39] Mouchtouris S and Kokkoris G 2021 A novel plasma fluid model for fast 2D calculations in capacitively coupled atmospheric pressure plasma jets *Plasma Sources Sci. Technol.* **30** 01LT01
[40] Ellerweg D, von Keudell A and Benedikt J 2012 *Plasma Sources Sci. Technol.* **21** 034019
[41] Beijer P A C, Sobota A, van Veldhuizen E M and Kroesen G M W 2016 *J. Phys. D: Appl. Phys.* **49** 104001
[42] Golda J, Held J and Schulz-von der Gathen V 2020 *Plasma Sources Sci. Technol.* **29** 025014
[43] Gorbanev Y, Golda J, Schulz-von der Gathen V and Bogaerts A 2019 *Plasma* **2** 316–27
[44] Niemi K, Schulz-von der Gathen V and Döbele H F 2001 *J. Phys. D: Appl. Phys.* **34** 2330–5
[45] Niemi K, Schulz-von der Gathen V and Döbele H F 2005 *Plasma Sources Sci. Technol.* **14** 375–86
[46] Schulze J, Derzsi A, Dittmann K, Hemke T, Meichsner J and Donkó Z 2011 *Phys. Rev. Lett.* **107** 275001
[47] Cosby P C 1993 *J. Chem. Phys.* **98** 9560–9
[48] Itikawa Y 2009 *J. Phys. Chem. Ref. Data* **38** 1–20
[49] Stafford D S and Kushner M J 2004 *J. Appl. Phys.* **96** 2451–65
[50] Turner M M 2015 *Plasma Sources Sci. Technol.* **25** 015003
[51] Mozetič M and Zalar A 2000 *Appl. Surf. Sci.* **158** 263–7
[52] Lopaev D V, Malykhin E M and Zyryanov S M 2010 *J. Phys. D: Appl. Phys.* **44** 015201
[53] Krištof J, Macko P and Veis P 2012 *Vacuum* **86** 614–19 13th Joint Conf., Štrbské Pleso, Slovakia, June 20–24, 2010 organized by the Slovak Vacuum Society in collaboration with the Vacuum Societies of Austria, Croatia, Czech Republic, Hungary and Slovenia
[54] Zhestkov B E, Kozlov S N and Alexandrov E N 2019 *High Temperature* **57** 329–34
[55] Golda J, Kogelheide F, Awakowicz P and Schulz-von der Gathen V 2019 *Plasma Sources Sci. Technol.* **28** 095023
[56] Klose S J *et al* 2020 *Plasma Sources Sci. Technol.* **29** 125018